



Varied alkyl chain functionalized organic dyes for efficient dye-sensitized solar cells: Influence of alkyl substituent type on photovoltaic properties

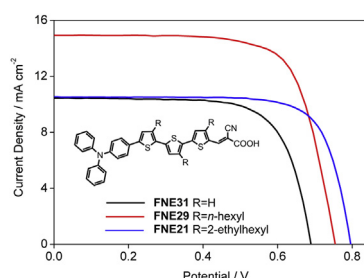
Quanyou Feng, Gang Zhou*, Zhong-Sheng Wang*

Department of Chemistry & Laboratory of Advanced Materials, Fudan University, 2205 Songhu Road, Shanghai 200438, PR China

HIGHLIGHTS

- Branched alkyl chains are superior in suppression of charge recombination in DSSC.
- Linear alkyl chains are better than branched alkyl chains in photocurrent generation.
- A power conversion efficiency of 8.12% was achieved for the DSSC based on **FNE29**.

GRAPHICAL ABSTRACT



ARTICLE INFO

Article history:

Received 29 October 2012

Received in revised form

25 February 2013

Accepted 11 March 2013

Available online 29 March 2013

Keywords:

Organic dye

Dye-sensitized solar cell

Charge recombination

Alkyl chain

Open-circuit photovoltage

ABSTRACT

Suppression of dye aggregation and interfacial charge recombination by appropriate structural modification of the sensitizers is crucial to improve the performance of dye-sensitized solar cells (DSSCs). In this article, linear alkyl chains, i.e., hexyl groups, and branched alkyl chains, i.e., 2-ethylhexyl groups, are introduced into a sensitizer with a terthiophene unit as conjugated bridge. The effects of the linear and branched alkyl chains on the photophysical, electrochemical properties and photovoltaic properties are investigated. By comparison, branched alkyl chains are superior to linear alkyl chains in suppression of intermolecular interactions and the electron recombination between the injected electrons and the electron acceptors in the electrolyte. Consequently, a more significant improvement of the open-circuit photovoltage can be achieved by the introduction of branched alkyl chains to the π -conjugated bridge of the organic dye in comparison to the incorporation of linear alkyl chains. Conversely, linear alkyl chains are better than branched alkyl chains in broadening photoresponse and hence photocurrent generation. As a result, a power conversion efficiency of 8.12% was achieved for the DSSC based on **FNE29** with linear alkyl chains.

© 2013 Elsevier B.V. All rights reserved.

1. Introduction

Dye-sensitized solar cells (DSSCs) have been extensively studied as potential photovoltaic devices due to their high power conversion efficiency (η) and relatively low cost [1]. Up to now, such cells

* Corresponding authors. Tel./fax: +86 21 5163 0345.

E-mail addresses: zhougang@fudan.edu.cn (G. Zhou), zs.wang@fudan.edu.cn (Z.-S. Wang).

employing mostly ruthenium polypyridyl complexes as sensitizers have achieved power conversion efficiencies above 11% under illumination of standard global air mass 1.5 (AM1.5G) simulated solar light [2]. However, the high cost of ruthenium, the difficulty of purification treatments and the low molar extinction coefficients may limit the large-scale application of this type sensitizer. As a result, metal-free organic dyes have attracted considerable attention for practical applications owing to their lower cost of production and better flexibility in terms of molecular tailoring [3].

Generally, organic sensitizers used for efficient DSSC devices are composed of three units which consist of a donor and acceptor connected by a π -conjugation bridge (D– π –A). In the last decade, many kinds of organic dyes with such configuration have been explored for DSSCs, including sensitizers based on thiophene [4], furan [5], selenophene [6], and pyrrole [7] derivatives, and impressive efficiency over 8% has been achieved in liquid electrolyte systems [4e,4h,8]. Recently, DSSC devices showing 12.3% efficiency have recently been achieved with zinc-porphyrin dye YD2–o–C8 cosensitized with an organic dye Y123 using cobalt-based electrolyte [9].

Despite the promising results obtained so far, many metal-free organic dyes have suffered from the dye aggregation problem [10], leading to molecules residing in the system not functionally attached to the TiO₂ surface and thus acting as light filters, which could have an adverse effect on the overall device efficiency [4e,11]. Another major hurdle in attaining higher solar-to-electric power conversion efficiency is the interfacial charge recombination losses [12]. Such interfacial charge carrier recombination may cause an open-circuit voltage (V_{oc}) reduction, hence decreasing the photoelectric conversion efficiency [13]. To control the π -stacked aggregation of organic dye molecules and those charge recombination processes, several kinds of additives, such as deoxycholic acid (DCA), have been introduced to coadsorb onto the semiconductor surface to prevent the intermolecular aggregation and improve the photovoltaic performance of DSSCs. We have clarified what intrinsic factors are responsible for the performance improvement and how they contribute to the enhancement quantitatively upon the coadsorption of DCA or its sodium salt [14]. In addition to the physical coadsorption on the TiO₂ surface, “chemical coadsorption” into the organic dye molecules was recently reported [4a,4i,15]. Linear alkyl chains were introduced into the dye skeleton, which not only prevented dye aggregation but also diminished the charge recombination between electrons and dye cations or acceptors in the electrolyte. However, the linear alkyl chain can significantly reduce the π – π interactions between adjacent molecules when the molecules are arranged in the direction coplanar to the π -conjugation plane, but cannot efficiently suppress the intermolecular π – π interactions when the molecules are arranged in the direction vertical to the π -conjugation plane. Therefore, when branched alkyl chains are incorporated into the π -bridge of dye molecules, the intermolecular π – π interactions can be reduced from two directions, and therefore higher V_{oc} is anticipated with the assistance of branched alkyl chains.

Herein, two types of alkyl substituents, i.e., linear alkyl chains (hexyl groups in **FNE29**) and branched alkyl chains (2-ethylhexyl groups in **FNE21**), are introduced into the terthiophene bridge of sensitizer **FNE31** (Fig. 1) to suppress the formation of dye aggregates and obstruct charge recombination in DSSCs. The influence of the branched 2-ethylhexyl chains and *n*-hexyl chains is

characterized by UV–vis absorption spectroscopy, photoluminescence (PL) spectroscopy, cyclic voltammetry (CV) and intensity-modulated photovoltage spectroscopy (IMVS). Moreover, effects of the branched alkyl chains and linear chains on photovoltaic performance and charge recombination dynamics in DSSCs were fully investigated.

2. Results and discussion

2.1. Synthesis and structural characterization

The synthetic approach to sensitizers **FNE21** and **FNE29** starting from the corresponding alkyl-functionalized terthiophene is depicted in Scheme 1. The compound **1b** was synthesized in a similar way as the preparation of **1a** [16]. After refluxing with a Vilsmeier reagent [17], the corresponding monoaldehyde-substituted derivatives **2a** and **2b** were obtained. Electron donor, triethylamine, was attached via C–H bond activation [18] and provided the precursors **3a** and **3b**. In the last step, the obtained precursors were converted to the corresponding sensitizers **FNE21** and **FNE29**, respectively, by Knoevenagel condensation [19] with cyanoacetic acid through refluxing acetonitrile in the presence of piperidine. It should be noted that a recently developed C–H bond activation was utilized to synthesize the precursor in moderate yield, which shortened the synthetic procedure by two steps. For comparison, **FNE31** is also synthesized according to reported method [4d]. The target compounds were characterized by ¹H NMR spectroscopy, ¹³C NMR spectroscopy, and mass spectroscopy, and were found to be consistent with the proposed structures. The obtained dyes are dark brown in the solid state and freely dissolve in dichloromethane (DCM) and tetrahydrofuran (THF) to produce a red solution.

2.2. Optical properties

The electronic absorption spectra of the three dyes in THF solutions are shown in Fig. 2. All of the dyes exhibit their major electronic absorption in the range of 400–600 nm in the visible region in THF solutions at room temperature, which can apparently be attributed to the intramolecular charge transfer (ICT) from the donor to the acceptor. The spectrum of **FNE31** displays a strong visible band at 478 nm ($\epsilon = 3.7 \times 10^4 \text{ M}^{-1} \text{ cm}^{-1}$). Moreover, when the concentration of **FNE31** increases from $5 \times 10^{-7} \text{ M}$ to 10^{-5} M , a bathochromic shift of 11 nm for the maximum absorption wavelength can be observed, which is obviously due to the strong aggregation tendency of the organic dye molecules, even at extremely low concentration condition. This is a well-known behavior for none substituted oligothiophene derivatives [4h,20]. Compared with **FNE31**, **FNE29** exhibits a hypsochromically shifted absorption maximum at 456 nm ($\epsilon = 3.4 \times 10^4 \text{ M}^{-1} \text{ cm}^{-1}$) with an intensity

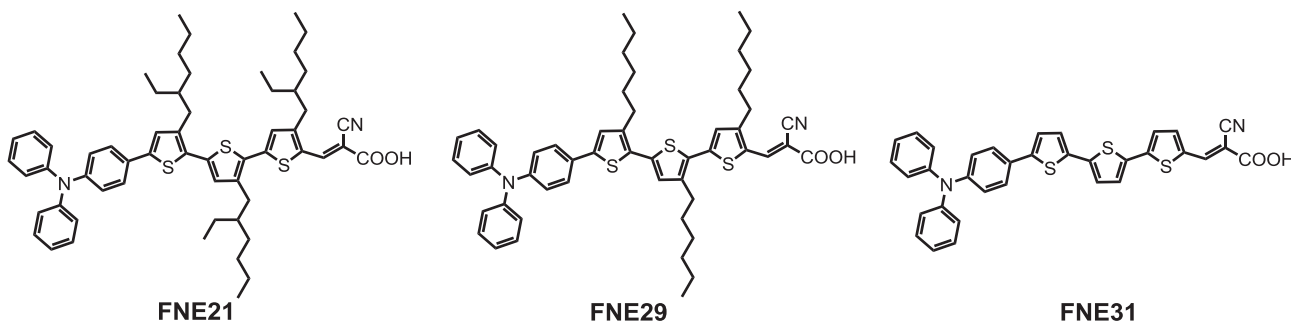
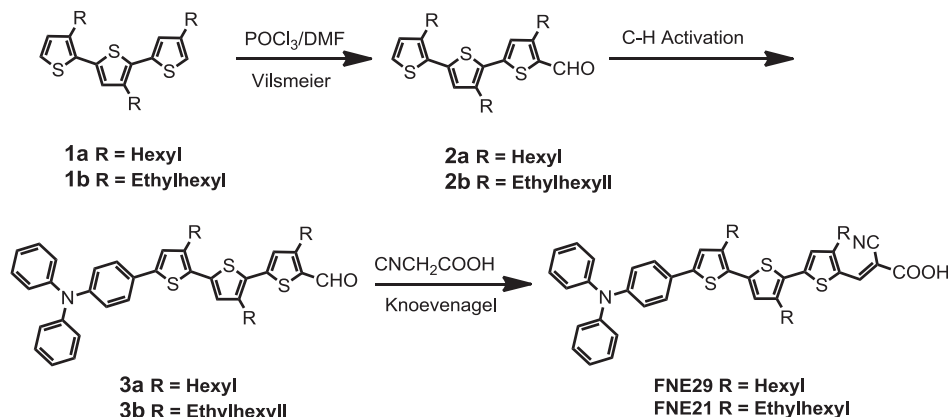


Fig. 1. Chemical structures of the dye molecules.

Scheme 1. Synthetic route for sensitizers **FNE21** and **FNE29**.

increase for the shoulder band, probably due to the interruption of π – π stacking by the hexyl groups. When the concentration of **FNE29** increases from 5×10^{-7} M to 10^{-5} M, a bathochromic shift of 2 nm can be found for **FNE29**, indicating that the introduction of linear alkyl chains inhibits the dye aggregation. Upon the introduction of ethyl group into the hexyl group, a further hypsochromic shift is observed for the absorption maximum of **FNE21** ($\lambda_{\max} = 454$ nm, $\epsilon = 3.0 \times 10^4$ M $^{-1}$ cm $^{-1}$), which further verifies the suppression of the aggregation by incorporation of branched alkyl chains. No absorption band shift can be clearly observed for **FNE21** when the concentration increases from 5×10^{-7} M to 10^{-5} M, which demonstrates that the branched alkyl chains can efficiently suppress the aggregation of the dye molecules and prevent the intermolecular π – π interactions.

The PL spectra of these dyes in THF solutions excited at 460 nm were also recorded and the corresponding data are also summarized in Table 1. As shown in Fig. 2, the maximum emission band locates at 589 nm for **FNE31**, 600 nm for **FNE29** and 611 nm for **FNE21**, respectively. Large Stokes shift (3943–5659 cm $^{-1}$) can be observed in all the three sensitizers, which is attributed to the charge transfer nature of the excited state [21]. Moreover, a more planar conformation of the excited state may also contribute to the Stokes shift [21]. Therefore, **FNE31** displays the smallest Stokes shift among all sensitizers due to its rigid and planar structure, while **FNE21** and **FNE29** exhibit larger Stokes shift due to the twisted structure conformation caused by the introduction of alkyl groups on the terthiophene unit. The fluorescence quantum yield of **FNE21**,

FNE29, and **FNE31** in THF solutions is measured to be 4.7%, 4.2%, and 2.1%, respectively. Obviously, upon the introduction of linear alkyl groups and further branched alkyl groups, the intermolecular interactions are suppressed and therefore the fluorescence quantum yield gradually increases.

When the dye molecules are attached to nanocrystalline TiO $_2$ films, a significant hypsochromic shift of the maximum absorption peak is observed for all dyes, as shown in Fig. 3, which can be owing to the deprotonation of the carboxylic acid. Such hypsochromic shift of the absorption spectra for organic dyes adsorbed on the TiO $_2$ films has also been observed in other metal-free organic dyes [4d,20c,22]. A more hypsochromic shift of the absorption maximum is observed for **FNE31** (62 nm) compared to **FNE29** (7 nm) and **FNE21** (13 nm). Furthermore, the absorption intensity decreased from 2.1 for **FNE31** to 1.3 for **FNE29** and 1.2 for **FNE21**. The presence of the alkyl chains prevent the adsorption of the dye molecules on the TiO $_2$ surface and therefore reduce the adsorption amount of the **FNE21** and **FNE29**. This is further proved by desorbing organic dyes from the TiO $_2$ surface. The surface concentration of **FNE31** is 2.9×10^{-8} mol cm $^{-2}$ μm^{-1} . With the introduction of alkyl chains into the dye molecules, the value decreased to 1.5×10^{-8} mol cm $^{-2}$ μm^{-1} for **FNE29** and further to 1.1×10^{-8} mol cm $^{-2}$ μm^{-1} for **FNE21**. This suggests that 2-ethylhexyl group, a branched alkyl chain, is more efficient for suppressing the intermolecular π – π stacking than hexyl group, a linear alkyl chain.

2.3. Electrochemical properties

Suitable highest occupied molecular orbital (HOMO) and lowest unoccupied molecular orbital (LUMO) energy levels of the dye molecules are required to match the redox potential of the triiodide/iodide couple and the conduction band edge of the nanocrystalline TiO $_2$ for efficient sensitizer regeneration and electron injection [23]. To determine the oxidation potential and evaluate the possibility of sensitizer regeneration, CV was carried out in a typical three-electrode electrochemical cell with TiO $_2$ films stained with sensitizer as the working electrode, Pt as the counter electrode and Ag/Ag $^+$ as the reference electrode dipped in a solution of tetrabutylammonium hexafluorophosphate (0.1 M) in water-free acetonitrile at a scan rate of 50 mV s $^{-1}$ at room temperature. All dyes exhibit one reversible oxidative wave at lower potential and one quasi-reversible oxidative wave at higher potential, which were attributed to the oxidation of the triphenylamine moiety and the oligothiophene segment, respectively (Fig. 4). The first half-wave potentials ($E_{1/2}$) for **FNE21**, **FNE29** and **FNE31**, which are taken as the HOMO levels of the dyes, was determined to be 1.13,

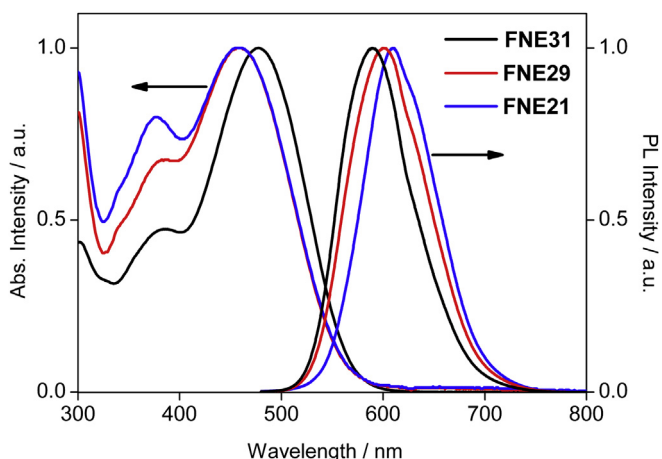


Fig. 2. UV–vis absorption and PL spectra of the sensitizers in THF solutions.

Table 1
Photophysical and electrochemical properties of the resulted sensitizers.

Dye	$\lambda_{\text{max}}^{\text{Abs}}$, nm ^a	ϵ , M ^{−1} cm ^{−1}	λ_{max} on TiO ₂ , nm	$\lambda_{\text{max}}^{\text{PL}}$, nm ^a	Φ_{PL} % ^b	Stokes shift, cm ^{−1}	HOMO, V ^c	E_{0-0} , eV	LUMO, V
FNE21	454	3.0×10^4	441	611	4.7	5659	1.13	2.17	−1.04
FNE29	456	3.4×10^4	449	600	4.2	5263	1.07	2.06	−0.99
FNE31	478	3.7×10^4	416	589	2.1	3943	1.11	2.11	−1.00

^a Absorption and PL spectra were measured in THF solutions.

^b Fluorescence quantum yield is measured relative to rhodamine B.

^c The potentials (vs. NHE) were calibrated with ferrocene.

1.07 and 1.11 V (vs. NHE), respectively. The close HOMO values for the three dyes are not difficult to be understood since they originate from the oxidation of the same triphenylamine moiety. All the HOMO values are more positive than I[−]/I₃[−] redox couples (~ 0.4 V vs. NHE), indicating that the reduction of the oxidized dyes with I[−] ions is thermodynamically feasible. Then LUMO energy level was estimated from equation (1),

$$\text{LUMO} = \text{HOMO} - \Delta E \quad (1)$$

where ΔE is the gap between the HOMO and LUMO levels and derived from the wavelength at 10% maximum absorption intensity for the dye-loaded TiO₂ film [3b]. Correspondingly, the LUMO energy levels of **FNE21**, **FNE29** and **FNE31** is −1.04, −0.99, and −1.00 V, respectively.

Furthermore, it was observed that the CV signal significantly decreased upon incorporation of hexyl chains into dye frames and further decreased upon switching from linear to branched alkyl substituents. As shown in Fig. 4, the decrease in current is much larger than the drop in adsorbed dye amount. One plausible explanation for this phenomenon is that alkyl chains attached to dye molecule act as spacers between dye molecules and thus prevent intermolecular electron hopping between the dye molecules [14]. This observation suggests that the branched 2-ethylhexyl chains can more effectively suppress the intermolecular interaction of dye molecules and weakens the electron hopping between two neighboring molecules than linear hexyl chains. It implies that the introduction of 2-ethylhexyl chains to the dye skeleton is favorable for suppressing the formation of dye aggregates and the recombination of electrons with acceptors in a DSSC device.

2.4. Theoretical approach

To gain insight into the geometrical and electronic properties of the resulted sensitizers, density functional calculations were conducted using the Gaussian 03 program package at the B3LYP/6-31G(d) level [24]. It can be clearly found from Fig. 5 that for all dyes, the HOMO is distributed along the donor part and the conjugated bridge while the LUMO is delocalized over the cyanoacrylic acid unit and the terthiophene spacer allowing significant charge separation within the dye and hence efficient electron injection upon photoexcitation. Furthermore, the presence of strong electron density relocation between HOMO and LUMO supports the occurrence of an intramolecular charge transfer transition in the UV–vis spectrum [25].

In addition, the coplanarity between the thiophene rings in the spacer is distinct. As shown in Fig. 5, the dihedral angle between the middle thiophene ring and the other one close to the cyanoacrylic acid unit is calculated to be 9°. However, due to the large steric effect introduced by the extended hexyl groups, **FNE29** displays a more twisted angle of 29°. This may perturb the conjugation efficiency of the chromophore and hence hypsochromically shift the absorption maximum wavelength, which is consistent with the experimental observation. Moreover, the introduction of 2-ethylhexyl groups induces a further twist of the oligothiophene unit and the dihedral angle is 41°. From the side views of the molecular geometry, hexyl groups separate the thiophene spacer only in one dimension, while 2-ethylhexyl groups isolate the thiophene rings in two dimensions, i.e., another perpendicular direction. Obviously, this result indicates that **FNE21** is much more efficient to suppress the aggregation among the dye molecules.

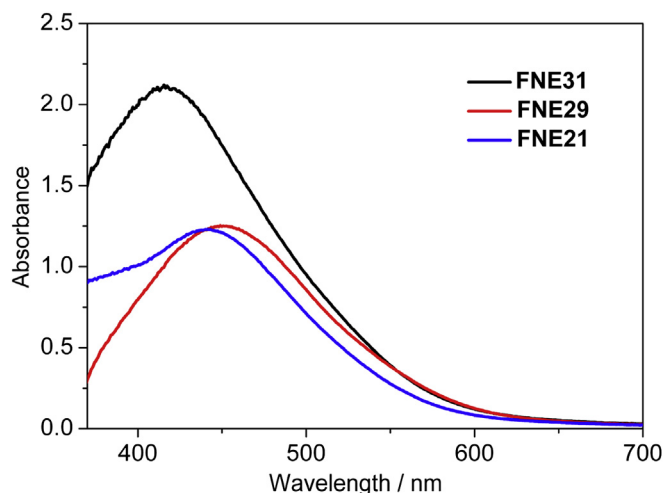


Fig. 3. UV–vis absorption spectra of the sensitizers on transparent titania films.

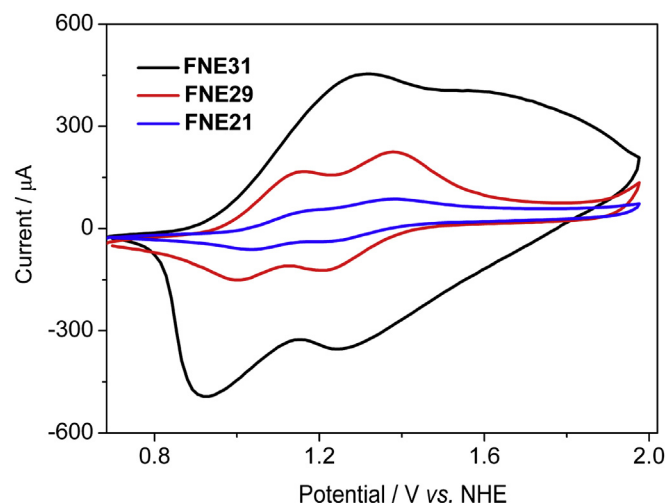


Fig. 4. Cyclic voltammograms of the dye-loaded TiO₂ films (0.25 cm², 6 µm thick).

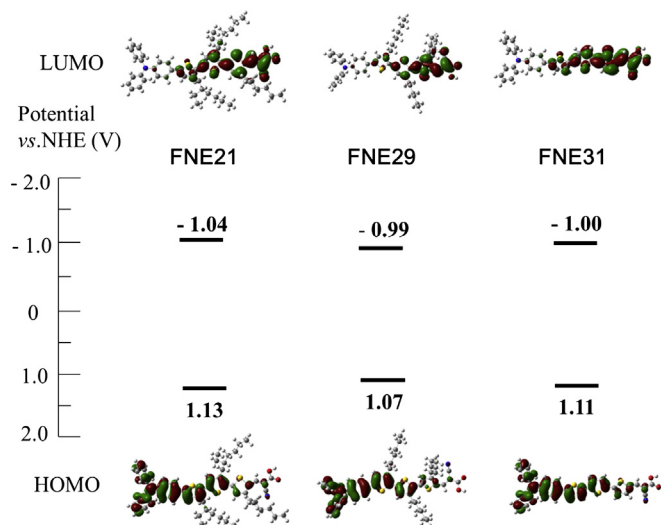


Fig. 5. Calculated frontier molecular orbitals and experimental energy level diagram of FNE21, FNE29, and FNE31.

2.5. DSSC performance

The DSSCs based on the resulted sensitizers were fabricated with an electrolyte containing 0.6 M 1,2-dimethyl-3-propylimidazolium iodide (DMPII), 0.1 M LiI, 0.05 M I₂, and 0.5 M 4-tert-butylpyridine (TPB) in acetonitrile. The corresponding current density–voltage (*J*–*V*) curves of the DSSCs were recorded under simulated AM1.5G irradiation (100 mW cm⁻²). As shown in Fig. 6, the DSSC based on FNE31 produced a short circuit photocurrent density (*J*_{sc}) of 10.44 mA cm⁻², an open circuit voltage (*V*_{oc}) of 689 mV, and a fill factor (*FF*) of 0.71, corresponding to a η of 5.11%. Under the same condition, upon the incorporation of linear hexyl groups on the terthiophene bridge, FNE29 based DSSC provided *J*_{sc} of 14.93 mA cm⁻², *V*_{oc} of 754 mV, and *FF* of 0.72, corresponding to η of 8.12%. It can be found that both *J*_{sc} and *V*_{oc} values significantly increased in comparison to those for FNE31 based DSSC, which leads to an improvement of the power conversion efficiency by 59%. Moreover, after the introduction of branched 2-ethylhexyl groups on the terthiophene bridge, the DSSC based on FNE21 produces a further enhanced *V*_{oc} value of 796 mV, which is 42 and 107 mV higher than that for the DSSCs based FNE29 or FNE31, respectively.

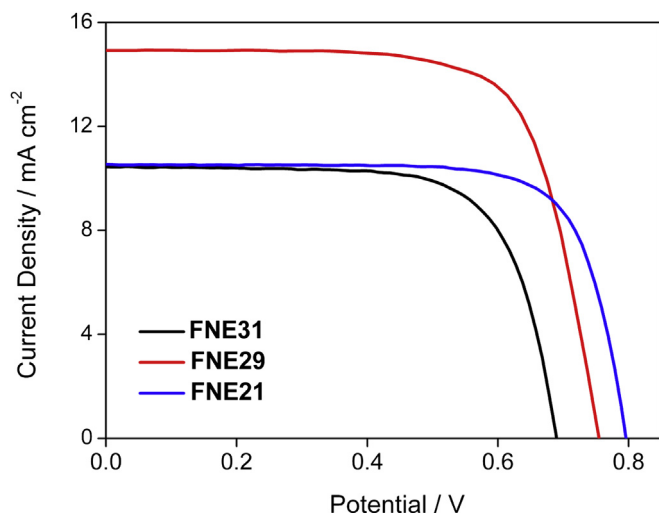


Fig. 6. *J*–*V* characteristics of DSSCs based on FNE21, FNE29, and FNE31.

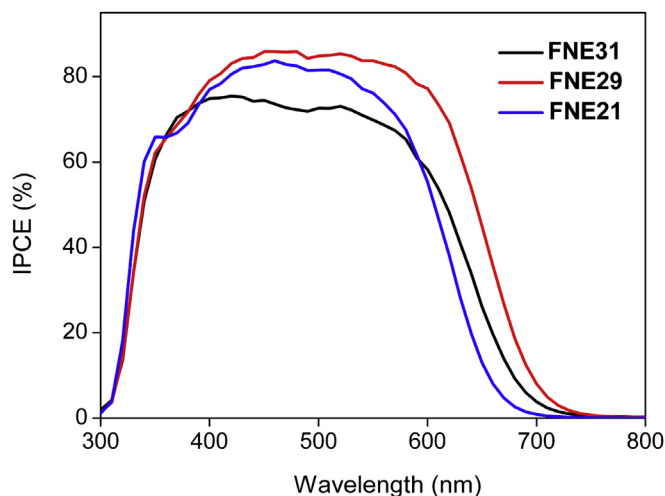


Fig. 7. IPCE action spectra for DSSCs based on FNE21, FNE29, and FNE31.

However, the *J*_{sc} value of FNE21 based DSSC dramatically decreased to 10.53 mA cm⁻², as compared with that for FNE29 based DSSC. Correspondingly, FNE21 based DSSC gave a η of 6.33%.

To understand the difference of the *J*_{sc} value, action spectra of the incident photon-to-current conversion efficiencies (IPCE) as a function of incident wavelength for the DSSCs based on the resulted sensitizers are recorded and shown in Fig. 7. It can be found that FNE31 based DSSC displays a maximum IPCE of 75% with a platform ranging from 350 to 550 nm. However, upon the introduction of alkyl chains into the dye molecules, although the dye amount on TiO₂ surface remarkably reduced, the maximum IPCE increased to 85% for FNE29 based DSSC. IPCE is a product of the electron injection efficiency, light-harvesting efficiency, and charge collection efficiency. For a dye-loaded film with thickness over 10 μ m, light harvesting efficiency can be considered to be 100%. Therefore, the significantly enhanced IPCE value is attributed to the introduced linear hexyl substituents, which interrupts the intermolecular interactions and thus improves the electron injection efficiency. Moreover, when replacing linear hexyl chains with branched 2-ethylhexyl chains in the sensitizer molecules, FNE21 based DSSC provided a comparable IPCE value with maximum of 83%. However, in comparison to FNE31 based DSSC, the DSSC based on FNE21 demonstrates a narrower IPCE spectrum due to the hypsochromic shift in the absorption spectrum of sensitizer FNE21 as compared with FNE31. Consequently, the integrated photocurrent for the DSSCs based on the three sensitizers are in the order of FNE21 \approx FNE31 < FNE29, which is consistent with the tendency of the *J*_{sc} values.

For another importance performance parameter (*V*_{oc}), it can be also found that the introduction of hexyl or 2-ethylhexyl improves the *V*_{oc} from 689 mV for FNE31 to 754 mV for FNE29 and 796 mV for FNE21, respectively. The branched alkyl chain is superior to the linear alkyl chain in improving *V*_{oc}. Since the generation of *V*_{oc} is related to the charge recombination in DSSCs, the significant *V*_{oc} improvements of 42 mV (FNE29) and 107 mV (FNE21) originate from the repression of the charge recombination. When hexyl groups are introduced into FNE31, the aggregation of the conjugation backbone is repressed in one dimension, which results in the retardation of the charge recombination and the 42 mV improvement of the *V*_{oc}. Furthermore, while 2-ethylhexyl groups are introduced into FNE31, the aggregation is blocked in two dimensions and the charge recombination rate is further slowed down, inducing the 107 mV improvement of the *V*_{oc}.

To further investigate the charge recombination, electron lifetime is evaluated since it is a judgment for the charge

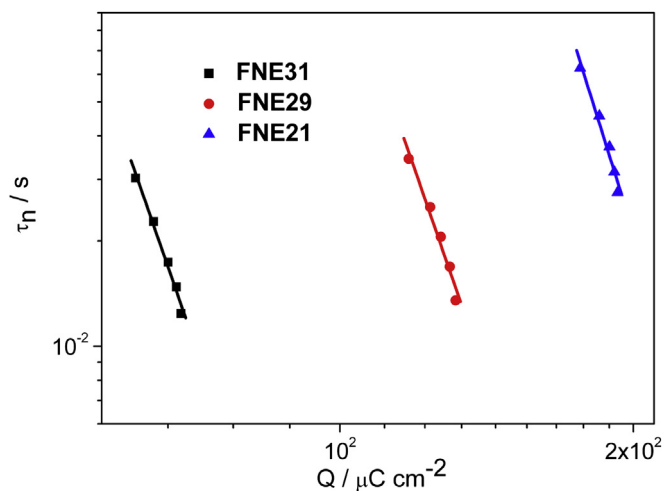


Fig. 8. Electron lifetime as a function of charge density at open circuit for DSSCs based on FNE21, FNE29, and FNE31.

recombination at open-circuit. To explore the change of the electron lifetime caused by the introduction of alkyl chains, charge extraction and IMVS measurements were carried out. Fig. 8 shows the electron lifetime (τ) as a function of charge density (Q), which was measured with charge extraction technique [26] under illumination of a white LED light for DSSCs using the resulted dyes as sensitizers. The electron lifetime was calculated by equation (2) [27]:

$$\tau = \frac{1}{2\pi f_{\min}} \quad (2)$$

where f_{\min} is the frequency at the top of the semicircle (f_{\min}) in IMVS. For all cases, electron lifetime decreased with increasing charge intensity following a power-law relation. At a fixed charge density, the electron lifetime for a DSSC based on FNE21 is larger than that of counterparts without alkyl chains and with linear hexyl chains. Consequently, the retarded charge recombination rate constant will reduce charge density at open circuit. When more charge is accumulated in TiO_2 , Fermi level moves upward and V_{oc} gets larger. These results explain the remarkable increase in V_{oc} from FNE31 to FNE29 (42 mV) and further to FNE21 (107 mV), and indicate that the charge recombination can be powerfully suppressed by the branched 2-ethylhexyl chains.

3. Conclusions

In summary, three organic dyes, i.e., FNE31 without alkyl chain; FNE29 with hexyl chains; and FNE21 with 2-ethylhexyl chains, have been synthesized and their photophysical, electrochemical and photovoltaic properties have been systematically investigated. It is found that the branched alkyl chains are superior to the linear alkyl chains in inhibiting dye aggregation and obstructing charge recombination. Therefore, the branched alkyl chain is more efficient to improve V_{oc} than the linear alkyl chain. However, the branched alkyl chains twist the conjugated backbone and hypsochromically shift the absorption band, resulting in a narrower IPCE curve and lower J_{sc} . Combining the two effects, a highest η of 8.12% was achieved for the DSSC based on FNE29 with linear alkyl chains. Therefore, to harvest more incident photons and thus improve the power conversion efficiency, our ongoing work is focused on further design of novel organic dyes with appropriate alkyl substituents to balance longer-wavelength absorption and efficient electron injection.

4. Experimental details

4.1. General information

^1H NMR (400 MHz) and ^{13}C NMR (100 MHz) spectra were measured on a Varian Mercury Plus-400 spectrometer. Data of ^1H NMR and ^{13}C NMR were recorded in CDCl_3 or CD_2Cl_2 solution. The chemical shifts were expressed in ppm downfield from tetramethylsilane (TMS). The splitting patterns are designated as follows: s (singlet); d (doublet); t (triplet); m (multiplet). The UV–vis absorption spectra of the dye solutions and the dye-loaded transparent films were recorded on a UV-3150PC spectrophotometer (Shimadzu). The PL spectra of the dye solutions were recorded on an RF-5301PC spectrofluorophotometer (Shimadzu) spectrophotometer. The fluorescence quantum yield is measured relative to rhodamine B [28]. Electrochemical redox potentials were obtained by cyclic voltammetry (CV) measurements, which were performed on a CH electrochemical workstation (CHI604D) using a typical three-electrode electrochemical cell in a solution of tetrabutylammonium hexafluorophosphate (0.1 M) in anhydrous acetonitrile at a scan rate of 50 mV s^{-1} at room temperature under nitrogen. Dye-adsorbed TiO_2 film (thickness: $6 \mu\text{m}$, size: 0.25 cm^2) on conductive glass was used as the working electrode, a Pt wire as the counter electrode, and an Ag/Ag^+ electrode as the reference in anhydrous acetonitrile. The potential of the reference electrode was calibrated with ferrocene, and all potentials mentioned in this work are against the normal hydrogen electrode (NHE).

4.2. Materials and reagents

All of the chemicals and reagents were purchased from commercial sources and used as received. Tetrahydrofuran (THF) was distilled from sodium benzophenone ketyl. Chloroform (CHCl_3) was distilled from CaH_2 . All reactions and manipulations were carried out under N_2 with the use of standard inert atmosphere and Schlenk techniques. The compound **1b** was synthesized in a similar way as the preparation of **1a** [16].

4.3. Syntheses

4.3.1. 3',3'',4-Tri-(*n*-hexyl)-[2,2',5',2'']terthiophene-5-carbaldehyde **2a**

Under a nitrogen atmosphere, compound **1a** (1.00 g, 2.00 mmol) and DMF (0.186 mL, 2.40 mmol) were dissolved in 30 mL chloroform. To this solution, phosphorus oxychloride (0.279 mL) was added slowly. The mixture was stirred for 20 min at room temperature and then heated to 90°C for 8 h. After cooling to room temperature, 30 mL of saturated sodium acetate solution was added to the dark red reaction solution with stirring for 20 min. The mixture was poured into ice water (50 mL) and neutralized ($\text{pH} = 7$) through the addition of sodium hydroxide solution. The product was extracted with DCM for three times. The combined organic solution was washed with sodium bicarbonate and sodium chloride solutions and dried over anhydrous sodium sulfate. After removal of the solvent, the residue was purified by flash column chromatography (silica gel, DCM:petroleum ether (PE) = 1:2). Orange oil **2a** was obtained with a yield of 46% (486 mg). ^1H NMR (400 MHz, CDCl_3 , δ): 10.00 (s, 1H), 7.19 (d, $J = 5.2 \text{ Hz}$, 1H), 7.03 (s, 1H), 6.96 (s, 1H), 6.94 (d, $J = 5.2 \text{ Hz}$, 1H), 2.94 (t, $J = 7.8 \text{ Hz}$, 2H), 2.76–2.83 (m, 4H), 1.61–1.72 (m, 6H), 1.31–1.41 (m, 18H), 0.88–0.91 (m, 9H); ^{13}C NMR (100 MHz, CDCl_3 , δ): 181.90, 153.65, 145.43, 142.60, 140.50, 136.46, 136.39, 130.48, 130.13, 129.66, 129.35, 128.32, 124.43, 31.89, 31.79, 31.67, 30.81, 30.46, 30.01, 29.57, 29.47, 29.44, 29.23, 28.71, 22.85, 22.79, 14.32, 14.30.

4.3.2. 3',3'',4-Tris(2-ethylhexyl)-[2,2',5',2'']terthiophene-5-carbaldehyde **2b**

Orange oil, yield, 3.21 g (63%). ^1H NMR (400 MHz, CDCl_3 , δ): 9.99 (s, 1H), 7.20 (d, $J = 5.2$ Hz, 1H), 7.00 (s, 1H), 6.93 (s, 1H), 6.91 (d, $J = 5.2$ Hz, 1H), 2.86 (d, $J = 7.2$ Hz, 2H), 2.75 (d, $J = 7.2$ Hz, 2H), 2.72 (d, $J = 7.2$ Hz, 2H), 1.65–1.69 (m, 3H), 1.24–1.38 (m, 24H), 0.83–0.93 (m, 18H); ^{13}C NMR (100 MHz, CDCl_3 , δ): 182.02, 152.79, 145.26, 141.67, 139.73, 137.20, 136.34, 131.01, 130.18, 129.23, 124.29, 41.82, 40.53, 40.34, 34.15, 33.70, 32.98, 32.80, 32.75, 32.05, 29.61, 29.03, 28.96, 28.92, 25.97, 23.30, 23.21, 14.36, 14.34, 11.04, 10.97.

4.3.3. 5''-(4-(Diphenylamino)phenyl)-3',3'',4-tri-*n*-hexyl-[2,2',5',2'']terthiophene-5-carbaldehyde **3a**

To a flask containing a mixture of K_2CO_3 (0.69 mmol, 95 mg), $\text{Pd}(\text{OAc})_2$ (0.009 mmol, 2.0 mg), $\text{PCy}_3 \cdot \text{HBF}_4$ (0.018 mmol, 7.0 mg), pivalic acid (0.138 mmol, 14 mg), 4-bromo-*N,N*-diphenylaniline (298 mg, 0.919 mmol) and **2a** (243 mg, 0.459 mmol) was added dry toluene (2 mL). The reaction mixture was then vigorously stirred at 105 °C for 16 h. The solution was then cooled to rt, diluted with CH_2Cl_2 and H_2O . The aqueous phase was extracted with CH_2Cl_2 . The organics were combined and dried over MgSO_4 , filtered, and evaporated under reduced pressure. The crude product was purified by silica gel column chromatography to afford red-orange oil **3a** in 59% yield (208 mg). ^1H NMR (400 MHz, CDCl_3 , δ): 10.00 (s, 1H), 7.44 (d, $J = 8.5$ Hz, 2H), 7.25–7.28 (m, 4H), 7.12 (d, $J = 7.8$ Hz, 4H), 7.02–7.06 (m, 6H), 6.99 (s, 1H), 2.94 (t, $J = 7.6$ Hz, 2H), 2.76–2.83 (m, 4H), 1.62–1.74 (m, 6H), 1.25–1.42 (m, 18H), 0.88–0.91 (m, 9H); ^{13}C NMR (100 MHz, CDCl_3 , δ): 181.86, 153.66, 147.68, 147.61, 145.49, 142.72, 142.54, 141.47, 136.63, 136.32, 129.57, 129.37, 128.88, 128.82, 128.21, 127.98, 126.56, 125.78, 125.64, 124.82, 123.71, 123.43, 31.93, 31.82, 31.69, 30.69, 30.46, 30.43, 30.07, 29.95, 29.51, 29.26, 28.73, 22.96, 22.89, 22.82, 14.39, 14.36, 14.33.

4.3.4. 5''-(4-(Diphenylamino)phenyl)-3',3'',4-tris(2-ethylhexyl)-[2,2',5',2'']terthiophene-5-carbaldehyde **3b**

Red-orange oil (100 mg, 36%). ^1H NMR (400 MHz, CDCl_3 , δ): 9.99 (s, 1H), 7.44 (d, $J = 8.6$ Hz, 2H), 7.24–7.28 (m, 4H), 7.11 (d, $J = 7.7$ Hz, 4H), 7.01–7.07 (m, 6H), 6.97 (s, 1H), 2.86 (d, $J = 7.2$ Hz, 2H), 2.76 (d, $J = 7.3$ Hz, 2H), 2.72 (d, $J = 7.2$ Hz, 2H), 1.65–1.71 (m, 3H), 1.25–1.39 (m, 24H), 0.85–0.93 (m, 18H); ^{13}C NMR (100 MHz, CDCl_3 , δ): 181.97, 152.82, 147.69, 147.63, 145.32, 142.40, 141.79, 140.67, 137.14, 136.51, 130.00, 129.76, 129.58, 129.34, 129.13, 128.04, 126.58, 126.19, 124.80, 123.77, 123.44, 41.85, 40.42, 40.34, 34.23, 34.13, 33.00, 32.84, 32.77, 29.98, 29.06, 29.00, 28.95, 26.00, 23.38, 23.34, 23.26, 14.45, 14.41, 14.39, 11.09, 11.05, 11.01.

4.3.5. 2-Cyano-3-[5''-(4-(diphenylamino)phenyl)-3',3'',4-tri-*n*-hexyl]-[2,2',5',2'']terthiophene]acrylic acid **FNE29**

To a flask containing a mixture of **3a** (856 mg, 1.11 mmol), cyanoacetic acid (239 mg, 2.81 mmol), chloroform (35 mL) and acetonitrile (35 mL) was added piperidine (0.2 mL). The mixture was refluxed at 120 °C for 6 h and allowed to cool to room temperature. The resulting mixture was washed with distilled water, brine, dried over with MgSO_4 and filtered. The solvent was removed by rotary evaporation. The residue was adsorbed on silica gel and purified by column chromatography ($\text{DCM} \rightarrow \text{DCM}:\text{CH}_3\text{OH} = 10:1$) to give a dark brown solid (522 mg, 56%). ^1H NMR (400 MHz, CD_2Cl_2 , δ): 8.32 (s, 1H), 7.29–7.31 (br, 2H), 7.17 (t, $J = 7.2$ Hz, 4H), 6.81–7.01 (m, 11H), 2.63–2.70 (m, 6H), 1.47–1.54 (m, 6H), 1.10–1.30 (m, 18H), 0.73–0.78 (m, 9H); ^{13}C NMR (100 MHz, CD_2Cl_2 , δ): 153.68, 140.89, 122.79, 122.71, 122.34, 121.21, 119.61, 118.94, 118.08, 116.80, 116.70, 35.11, 33.57, 25.33, 25.31, 25.22, 25.20, 23.97, 23.77, 23.73, 23.69, 23.66, 23.64, 23.61, 23.59, 23.58, 23.29, 23.22, 22.86, 22.83, 22.77, 22.71, 22.62, 16.13, 14.69, 14.54, 14.47, 13.90, 13.86, 13.81, 11.30. ESI-Mass: m/z 837.4.

4.3.6. 2-Cyano-3-[5''-(4-(diphenylamino)phenyl)-3',3'',4-tris(2-ethylhexyl)-[2,2',5',2'']terthiophene]acrylic acid **FNE21**

Dark brown solid (66 mg, 39%). ^1H NMR (400 MHz, CD_2Cl_2 , δ): 8.37 (s, 1H), 7.39 (d, $J = 8.5$ Hz, 2H), 7.20 (t, $J = 7.8$ Hz, 4H), 6.94–7.05 (m, 11H), 2.74 (d, $J = 7.2$ Hz, 2H), 2.66–2.69 (m, 4H), 1.51–1.68 (m, 3H), 1.18–1.34 (m, 24H), 0.79–0.84 (m, 18H); ^{13}C NMR (100 MHz, CD_2Cl_2 , δ): 156.26, 147.80, 147.58, 146.35, 145.20, 143.04, 142.52, 141.19, 137.35, 132.61, 130.25, 130.21, 129.79, 129.72, 129.69, 129.67, 129.63, 129.58, 129.54, 129.49, 129.08, 128.65, 127.76, 126.44, 126.34, 124.95, 124.93, 124.84, 123.57, 123.51, 123.48, 123.43, 116.31, 109.72, 34.49, 34.08, 33.53, 32.77, 32.69, 32.49, 31.34, 30.14, 29.91, 29.87, 29.82, 29.76, 29.59, 28.95, 28.93, 28.88, 28.81, 28.78, 25.99, 25.96, 25.77, 23.32, 23.30, 23.20, 22.92, 14.15, 14.13, 14.09, 10.87, 10.77, 10.58. ESI-Mass: m/z 921.4.

4.4. Fabrication of dye-sensitized solar cells

Fluorine-doped SnO_2 glass (14 Ω/sq , Nippon Sheet Glass) substrates were cleaned in a detergent solution by an ultrasonic bath, washed with acetone, and water, then dried using N_2 current. Nanocrystalline TiO_2 films (thickness: 12 μm , size: 0.25 cm^2) were prepared using screen printing technique [29], followed by sintering at 450 °C under an air flow. After cooling, the TiO_2 films were impregnated in a 0.05 M aqueous TiCl_4 solution for 30 min at 70 °C and then rinsed with deionized water. The TiCl_4 -treated TiO_2 films were annealed at 450 °C for 30 min and then cooled to 100 °C before immersed into the dye solution (0.3 mM in chloroform:ethanol = 7:3) for 16 h to allow the dye to adsorb to the TiO_2 surface. After the adsorption of the dyes, the electrodes were rinsed with chloroform and acetonitrile. The resulting photo-electrode and Pt-counter electrodes were assembled into a sealed sandwich solar cell with a thermoplastic frame (Surlyn 30 μm thick). Redox electrolyte (0.6 M 1,2-dimethyl-3-*n*-propylimidazolium iodide, 0.1 M LiI, 0.05 M I_2 , and 0.5 M 4-*tert*-butylpyridine in acetonitrile) was introduced through a hole in the counter electrode via suction through another drilled hole. Finally, the two holes were sealed using additional hot melt Surlyn film covered with a thin glass slide.

4.5. Photovoltaic measurements

The current density–voltage (J – V) characteristics of the DSSCs were measured by recording J – V curves using a Keithley 2400 source meter under the illumination of AM1.5G simulated solar light coming from a solar simulator (Oriel-91193 equipped with a 1000 W Xe lamp and an AM1.5 filter). The DSSCs were fully covered with a black mask with an aperture area of 0.2304 cm^2 during measurements. The incident light intensity was calibrated with a standard silicon solar cell (Newport 91150). The electron lifetimes were measured with intensity modulated photovoltage spectroscopy (IMVS) [30], whereas charge densities at open-circuit were measured using charge extraction technique [26]. IMVS analysis and charge extraction were carried out on an electrochemical workstation (Zahner XPOT, Germany), which includes a white light emitting diode and corresponding control system. The intensity-modulated spectra were measured at room temperature with light intensity ranging from 20 to 120 W m^{-2} , in modulation frequency ranging from 0.1 Hz to 10 kHz, and with modulation amplitude less than 5% of the light intensity. Three identical devices were tested in each case with standard deviation less than 5%. Action spectra of the incident monochromatic photon-to-electron conversion efficiency (IPCE) for the solar cells were obtained with an Oriel-74125 system (Oriel Instruments). The intensity of monochromatic light was measured with a Si detector (Oriel-71640).

Acknowledgments

This work was financially supported by the National Basic Research Program (2011CB933302) of China, the National Natural Science Foundation of China (90922004, 50903020, 51273045, and 20971025), Shanghai Pujiang Project (11PJ1401700), Shanghai Leading Academic Discipline Project (B108), and Jiangsu Major Program (BY2010147).

References

- [1] B. O'Regan, M. Grätzel, *Nature* 353 (1991) 737–740.
- [2] (a) M.K. Nazeeruddin, F. De Angelis, S. Fantacci, A. Selloni, G. Viscardi, P. Liska, S. Ito, B. Takeru, M.G. Grätzel, *J. Am. Chem. Soc.* 127 (2005) 16835–16847; (b) M. Grätzel, *J. Photochem. Photobiol. C – Photochem. Rev.* 4 (2003) 145–153; (c) F. Gao, Y. Wang, D. Shi, J. Zhang, M. Wang, X. Jing, R. Humphry-Baker, P. Wang, S.M. Zakeeruddin, M. Grätzel, *J. Am. Chem. Soc.* 130 (2008) 10720–10728; (d) C.Y. Chen, M.K. Wang, J.Y. Li, N. Pootrakulchote, L. Alibabaei, C.H. Ngoc-le, J.D. Decoppet, J.H. Tsai, C. Grätzel, C.G. Wu, S.M. Zakeeruddin, M. Grätzel, *ACS Nano* 3 (2009) 3103–3109.
- [3] (a) A. Mishra, M.K.R. Fischer, P. Bäuerle, *Angew. Chem. Int. Ed.* 48 (2009) 2474–2499; (b) A. Hagfeldt, G. Boschloo, L. Sun, L. Kloo, H. Pettersson, *Chem. Rev.* 110 (2010) 6595–6663.
- [4] (a) H. Choi, C. Baik, S.O. Kang, J. Ko, M.S. Kang, M.K. Nazeeruddin, M. Grätzel, *Angew. Chem. Int. Ed.* 47 (2008) 327–330; (b) J.H. Yum, D.P. Hagberg, S.J. Moon, K.M. Karlsson, T. Marinado, L.C. Sun, A. Hagfeldt, M.K. Nazeeruddin, M. Grätzel, *Angew. Chem. Int. Ed.* 48 (2009) 1576–1580; (c) W.H. Liu, L.C. Wu, C.H. Lai, C.H. Lai, P.T. Chou, Y.T. Li, C.L. Chen, Y.Y. Hsu, Y. Chi, *Chem. Commun.* (2008) 5152–5154; (d) K.R. Justin Thomas, Y.-C. Hsu, J.T. Lin, K.-M. Lee, K.-C. Ho, C.-H. Lai, Y.-M. Cheng, P.-T. Chou, *Chem. Mater.* 20 (2008) 1830–1840; (e) Z.-S. Wang, N. Koumura, Y. Cui, M. Takahashi, H. Sekiguchi, A. Mori, T. Kubo, A. Furube, K. Hara, *Chem. Mater.* 20 (2008) 3993–4003; (f) J.-i. Nishida, T. Masuko, Y. Cui, K. Hara, H. Shibuya, M. Ihara, T. Hosoyama, R. Goto, S. Mori, Y. Yamashita, *J. Phys. Chem. C* 114 (2010) 17920–17925; (g) M.F. Xu, R.Z. Li, N. Pootrakulchote, D. Shi, J. Guo, Z.H. Yi, S.M. Zakeeruddin, M. Grätzel, P. Wang, *J. Phys. Chem. C* 112 (2008) 19770–19776; (h) S. Kim, J.K. Lee, S.O. Kang, J. Ko, J.H. Yum, S. Fantacci, F. De Angelis, D. Di Censo, M.K. Nazeeruddin, M. Grätzel, *J. Am. Chem. Soc.* 128 (2006) 16701–16707; (i) N. Koumura, Z.-S. Wang, S. Mori, M. Miyashita, E. Suzuki, K. Hara, *J. Am. Chem. Soc.* 128 (2006) 14256–14257; (j) H. Qin, S. Wenger, M. Xu, F. Gao, X. Jing, P. Wang, S.M. Zakeeruddin, M. Grätzel, *J. Am. Chem. Soc.* 130 (2008) 9202–9203; (k) Y. Liang, B. Peng, J. Liang, Z. Tao, J. Chen, *Org. Lett.* 12 (2010) 1204–1207. (l) H.-Y. Yang, Y.-S. Yen, Y.-C. Hsu, H.-H. Chou, J.T. Lin, *Org. Lett.* 12 (2009) 16–19.
- [5] (a) S.H. Kim, H.W. Kim, C. Sakong, J. Namgoong, S.W. Park, M.J. Ko, C.H. Lee, W.I. Lee, J.P. Kim, *Org. Lett.* 13 (2011) 5784–5787; (b) J.T. Lin, P.-C. Chen, Y.-S. Yen, Y.-C. Hsu, H.-H. Chou, M.-C.P. Yeh, *Org. Lett.* 11 (2008) 97–100.
- [6] R.Z. Li, X.J. Lv, D. Shi, D.F. Zhou, Y.M. Cheng, G.L. Zhang, P. Wang, *J. Phys. Chem. C* 113 (2009) 7469–7479.
- [7] Y.-S. Yen, Y.-C. Hsu, J.T. Lin, C.-W. Chang, C.-P. Hsu, D.-J. Yin, *J. Phys. Chem. C* 112 (2008) 12557–12567.
- [8] (a) T. Horiuchi, H. Miura, K. Sumioka, S. Uchida, *J. Am. Chem. Soc.* 126 (2004) 12218–12219; (b) S. Ito, H. Miura, S. Uchida, M. Takata, K. Sumioka, P. Liska, P. Comte, P. Péchy, M. Grätzel, *Chem. Commun.* (2008) 5194–5196; (c) S. Ito, S.M. Zakeeruddin, R. Humphry-Baker, P. Liska, R. Charvet, P. Comte, M.K. Nazeeruddin, P. Péchy, M. Takata, H. Miura, S. Uchida, M. Grätzel, *Adv. Mater.* 18 (2006) 1202–1205; (d) H.N. Tsao, C. Yi, T. Moehl, J.-H. Yum, S.M. Zakeeruddin, M.K. Nazeeruddin, M. Grätzel, *ChemSusChem* 4 (2011) 591–594; (e) W.D. Zeng, Y.M. Cao, Y. Bai, Y.H. Wang, Y.S. Shi, M. Zhang, F.F. Wang, C.Y. Pan, P. Wang, *Chem. Mater.* 22 (2010) 1915–1925.
- [9] A. Yella, H.W. Lee, H.N. Tsao, C. Yi, A.K. Chandiran, M.K. Nazeeruddin, E.W.G. Diao, C.Y. Yeh, S.M. Zakeeruddin, M. Grätzel, *Science* 334 (2011) 629–634.
- [10] (a) H. Choi, I. Raabe, D. Kim, F. Teocoli, C. Kim, K. Song, J.H. Yum, J. Ko, M.K. Nazeeruddin, M. Grätzel, *Chem. Eur. J.* 16 (2010) 1193–1201; (b) D. Liu, R.W. Fessenden, G.L. Hug, P.V. Kamat, *J. Phys. Chem. B* 101 (1997) 2583–2590.
- [11] X.F. Wang, O. Kitao, H.S. Zhou, H. Tamiaki, S. Sasaki, *J. Phys. Chem. C* 113 (2009) 7954–7961.
- [12] A. Kongkanand, R. Martínez Domínguez, P.V. Kamat, *Nano Lett.* 7 (2007) 676–680.
- [13] (a) Y. Diamant, S.G. Chen, O. Melamed, A. Zaban, *J. Phys. Chem. B* 107 (2003) 1977–1981; (b) K.M.P. Bandaranayake, M.K.I. Senevirathna, P.M.G.M.P. Weligamuwa, K. Tennakone, *Coord. Chem. Rev.* 248 (2004) 1277–1281; (c) R. Gao, L.D.O. Wang, B.B. Ma, C. Zhan, Y. Qiu, *Langmuir* 26 (2010) 2460–2465.
- [14] X.M. Ren, Q.Y. Feng, G. Zhou, C.H. Huang, Z.-S. Wang, *J. Phys. Chem. C* 114 (2010) 7190–7195.
- [15] (a) K.J. Jiang, N. Masaki, J.B. Xia, S. Noda, S. Yanagida, *Chem. Commun.* (2006) 2460–2462; (b) C.Y. Chen, S.J. Wu, C.G. Wu, J.G. Chen, K.C. Ho, *Angew. Chem. Int. Ed.* 45 (2006) 5822–5825; (c) F.F. Gao, Y. Wang, J. Zhang, D. Shi, M.K. Wang, R. Humphry-Baker, P. Wang, S.M. Zakeeruddin, M. Grätzel, *Chem. Commun.* (2008) 2635–2637; (d) S. Kim, D. Kim, H. Choi, M.S. Kang, K. Song, S.O. Kang, J. Ko, *Chem. Commun.* (2008) 4951–4953.
- [16] S. Gondo, Y. Goto, M. Era, *Mol. Cryst. Liq. Cryst.* 470 (2007) 353–358.
- [17] V.J. Majo, P.T. Perumal, *J. Org. Chem.* 61 (1996) 6523–6525.
- [18] D.J. Schipper, K. Fagnou, *Chem. Mater.* 23 (2011) 1594–1600.
- [19] S. Wada, H. Suzuki, *Tetrahedron Lett.* 44 (2003) 399–401.
- [20] (a) R. Chen, X. Yang, H. Tian, X. Wang, A. Hagfeldt, L. Sun, *Chem. Mater.* 19 (2007) 4007–4015; (b) S. Kim, H. Choi, D. Kim, K. Song, S.O. Kang, J. Ko, *Tetrahedron* 63 (2007) 9206–9212; (c) K. Hara, Z.-S. Wang, T. Sato, A. Furube, R. Katoh, H. Sugihara, Y. Dan-Oh, C. Kasada, A. Shinpo, S. Suga, *J. Phys. Chem. B* 109 (2005) 15476–15482.
- [21] H.-H. Chou, Y.-C. Chen, H.-J. Huang, T.-H. Lee, J.T. Lin, C. Tsai, K. Chen, *J. Mater. Chem.* 22 (2012) 10929–10938.
- [22] (a) T. Kitamura, M. Ikeda, K. Shigaki, T. Inoue, N.A. Anderson, X. Ai, T. Lian, S. Yanagida, *Chem. Mater.* 16 (2004) 1806–1812; (b) D.P. Hagberg, T. Edvinsson, T. Marinado, G. Boschloo, A. Hagfeldt, L.C. Sun, *Chem. Commun.* (2006) 2245–2247; (c) S.-L. Li, K.-J. Jiang, K.-F. Shao, L.-M. Yang, *Chem. Commun.* (2006) 2792–2794.
- [23] X. Lu, Q. Feng, T. Lan, G. Zhou, Z.-S. Wang, *Chem. Mater.* 24 (2012) 3179–3187.
- [24] M.J. Frisch, G.W. Trucks, H.B. Schlegel, G.E. Scuseria, M.A. Robb, J.R. Cheeseman, J.A. Montgomery, T. Vreven, K.N. Kudin, J.C. Burant, J.M. Millam, S.S. Iyengar, J. Tomasi, V. Barone, B. Mennucci, M. Cossi, G. Scalmani, N. Rega, G.A. Petersson, H. Nakatsuji, M. Hada, M. Ehara, K. Toyota, R. Fukuda, J. Hasegawa, M. Ishida, T. Nakajima, Y. Honda, O. Kitao, H. Nakai, M. Klene, X. Li, J.E. Knox, H.P. Hratchian, J.B. Cross, V. Bakken, C. Adamo, J. Jaramillo, R. Gomperts, R.E. Stratmann, O. Yazyev, A.J. Austin, R. Cammi, C. Pomelli, J.W. Ochterski, P.Y. Ayala, K. Morokuma, G.A. Voth, P. Salvador, J.J. Dannenberg, V.G. Zakrzewski, S. Dapprich, A.D. Daniels, M.C. Strain, O. Farkas, D.K. Malick, A.D. Rabuck, K. Raghavachari, J.B. Foresman, J.V. Ortiz, Q. Cui, A.G. Baboul, S. Clifford, J. Cioslowski, B.B. Stefanov, G. Liu, A. Liashenko, P. Piskorz, I. Komaromi, R.L. Martin, D.J. Fox, T. Keith, A.L. M.A. Laham, C.Y. Peng, A. Nanayakkara, M. Challacombe, P.M.W. Gill, B. Johnson, W. Chen, M.W. Wong, C. Gonzalez, J.A. Pople, *Gaussian 03, Revision c.02*, Gaussian, Inc., Wallingford, CT, 2004.
- [25] M.K.R. Fischer, S. Wenger, M.K. Wang, A. Mishra, S.M. Zakeeruddin, M. Grätzel, P. Bäuerle, *Chem. Mater.* 22 (2010) 1836–1845.
- [26] N.W. Duffy, L.M. Peter, R.M.G. Rajapakse, K.G.U. Wijayantha, *J. Phys. Chem. B* 104 (2000) 8916–8919.
- [27] R. Kern, R. Sastrawan, J. Ferber, R. Stangl, J. Luther, *Electrochim. Acta* 47 (2002) 4213–4225.
- [28] K.G. Casey, E.L. Quitevis, *J. Phys. Chem.* 92 (1988) 6590–6594.
- [29] Z.-S. Wang, H. Kawauchi, T. Kashima, H. Arakawa, *Coord. Chem. Rev.* 248 (2004) 1381–1389.
- [30] G. Schlichthorl, S.Y. Huang, J. Sprague, A.J. Frank, *J. Phys. Chem. B* 101 (1997) 8141–8155.